Iranian Journal of Medical Physics

ijmp.mums.ac.ir

Validation of Monte Carlo Model for Dose Evaluation outside the Treatment Field for Siemens 6MV Beam

Dina Mohamed Sinousy[1*], Ehab Marouf Attalla[2], Ibrahim Hassan Fathy[3], Fathi Ahmed Elhussiny[4], Ahmed Farouk Elmekawy[4]

1. Mit Ghamr Oncology Center,Egypt
2. National Cancer Institute; Cairo University; Egypt
3. Faculty of Science; Physics Department; Cairo University; Egypt
4. Faculty of Science; Physics Department; Tanta University, Egypt

ARTICLE INFO

Article type:
Original Paper

Article history:
Received: Sep 02, 2019
Accepted: Nov 26, 2019

Keywords:
Out-of-Field Dose
Monte Carlo Method
Linear Accelerator
Radiotherapy

ABSTRACT

Introduction: There has been a concern about the unintended doses to critical structures outside the treatment field due to the increased risk of radiation-induced second cancer following radiotherapy treatments. Today, Monte Carlo (MC) simulation is considered the most accurate method for dose calculations in different domains of medical physics.

Material and Methods: The Geant4 Application for Tomographic Emission (GATE) code was used to create an MC model of 6MV Siemens Primus linac. Measurements were taken in a water phantom using an ion chamber to validate the MC model. Dose profiles outside the treatment field at 1.5 (d_{max}), 5.0 and10.0 cm depths for field sizes from 5×5 to 20×20 cm^2 were measured in the present study. Out-of-field percentage depth dose (PDD) curves at 0.0, 5.0, and 7.5 cm off axis for field size 10×10 cm^2 were investigated for both measurements and simulation. However out-of-field PDDs from 10 to 15 cm off axis for field size 10×10 cm^2 were studied only by simulation.

Results: The comparisons showed agreement between the measured and simulated doses for the out-of-field profiles along the in-plane direction for all considered field sizes and depths, as well as for the PDDs at 0.0 and 5.0 cm off axis, but with less agreement at 7.5 cm off axis. All the simulated out-of-field PDDs at distances ≥ 10 cm off axis had similar trend shapes.

Conclusion: The developed MC model is considered a good representation of 6 MV Siemens Primus linac for the out-of-field dose calculation in lieu of measurements.

► *Please cite this article as:*
Sinousy DM, Attalla EM, Fathy IH, Elhussiny FA, Elmekawy AF. Validation of Monte Carlo Model for Dose Evaluation Outside the Treatment Field for Siemens 6MV Beam. Iran J Med Phys 2020; 17: 410-420.10.22038/ijmp.2019.42881.1646.

Introduction

The principal concept of radiation therapy is delivering the optimum radiation dose to the tumor while decreasing the dose to the healthy tissues that surrounded the tumor. In radiation therapy, organs distant from the tumor may receive low doses and consequently are not considered part of the treatment planning. Nevertheless, it has long been notable that such a comparatively low level of doses outside the field of treatment may be detrimental to the patient and probably result in the induction of second cancers (SCs) in patients after the radiotherapy course [1].

The accurate knowledge of the dose profile (DP) outside the treatment field from radiotherapy is necessary for the evaluation of various potential situations. For example, out-of-field radiation is of special interest in the treatment of pregnant patients, because even at received doses as low as 5cGy, the fetus is particularly vulnerable [2]. On a larger scale, the low doses of radiation may induce late effects in patients, such as cataracts [3], heart disease, stroke, digestive and respiratory diseases [4] as well as secondary malignancies [5].

Elgendy et al. [6] calculated the induced SC risk values in left breast cancer for various radiotherapy techniques using three-dimensional conformal radiotherapy (3DCRT) without external wedges and intensity-modulated radiotherapy (IMRT) plans. They concluded that equivalent doses for organs at risk were higher in IMRT than tangential beams. In addition, Sungkoo et al. [7] determined the SC risk values to the out-of-field organs for the head, neck, chest, and prostate cases using 3DCRT. They concluded that the SC risk was fundamentally affected by nominal cancer risk coefficients as the equivalent doses to the out-of-field organs were very low and similar.

There are currently a few methods available for the determination of the out-of-field doses. The most

**Corresponding Author:* Tel: 00201007163472; E-mail: Mohamed201@gmail.com

common method is dose measurements in phantoms; however, but the measurements are very time-consuming and require special measuring equipment. Furthermore, the measurement of the out-of-field doses experimentally in organs from radiation treatments demands a suitable anthropomorphic phantom in addition to the tedious placement of various calibrated dosimeters in corresponding cavity locations inside it for each different case. Conversely, computational techniques, such as the Monte Carlo (MC) model, are alternatives to the measurements for the determination of the out-of-field doses.

The MC model is the most mathematical accurate method for the calculation of dose distributions, especially inside inhomogeneous materials where the electron transport effects cannot be accurately calculated by the conventional methods using the deterministic algorithms [8]. In the MC model, the detailed modeling of the head for a linear accelerator (i.e., linac) can be used to obtain several parameters, such as mean energy distribution and fluence distribution. The results of several studies have confirmed that every linac has its own unique specifications [9-11]. The MC models can accurately calculate the out-of-field doses, provided that the model should be initially validated in this regard [12].

There are several MC codes that have been used to calculate the out-of-field doses, including: Monte Carlo N-Particle Transport code (MCNP), MCNP extended (MCNPX). In addition to , extended and improved version of the Electron Gamma Shower (EGS) software package originally developed by National Research Council (EGSnrc), Application for Tomographic Emission (Geant4), and FLUktuierende KAskade is a closed-source semi-integrated Monte Carlo simulation package for the interaction and transport of particles and nuclei in matter (FLUKA). The Geant4 /GATE code is the utilized code in the present study. For medical physics applications, the Geant4 code has some advantages over other codes. The factors affecting the choice of an MC code are the accuracy, computational efficiency, convenience of use, flexibility for the simulation of complex detector geometries, experimental arrangements, support as well as maintenance.

The Geant4/GATE has certain advantages for dosimetry calculations over other MC codes. Due to the modularity of Geant4, the users can load, use, and adjust only the required components. It includes a large variety of physics models, such as photo-nuclear reactions, which play an essential role in higher energy external beam dosimetry. In addition, the design and accessibility of Geant4 enable a simple conception for the used physics models. Geant4 exhibits the probabilities to trace extremely short steps permitting the calculations for micro-dosimetry. It can even be utilized for low energy medical applications for electron and photon sources; therefore, it can track extremely low energy particles down to 250eV while allowing for any involved hadronic processes. The disadvantages related to Geant4/GATE are the shortage of tracking the advanced particle modules, such as boundary crossing models, for electron transport simulations and advanced various scattering algorithms. Another disadvantage of the Geant4/GATE is associated with the simulation time efficiency where it suffers from the lack of advanced variance reduction techniques, such as those present in other codes, including EGSnrc and MCNP [13].

GATE /Geant4 is an application that currently plays a key role in the design of many medical imaging devices, optimization of acquisition protocols, and dose calculations for radiotherapy. The GATE has been developed as an open-source software package [14] by the international Open GATE collaboration for nuclear medicine simulation with an original focus on positron emission tomography (PET) and single-photon emission computed tomography (SPECT) imaging [15-16].

This platform; supporting the Geant4 MC toolkit is considered a cooperative development by researchers from many international establishments [17]. These researchers have suggested to create a simulation on the premise of easy macro-commands rather than handling difficult C++ syntaxes.

The current study was performed to validate a new MC model for the calculation of the out-of-field dose using the Geant4/ GTAE code for various distances at and away from the edge of the treatment field for a Siemens Primus linac (Siemens AG, Erlangen, Germany) operated at 6 MV. The validation involved photon doses only without any concerns about neutrons because the used low-energy 6 MV photon beam does not produce any significant neutrons.

Materials and Methods

Monte Carlo model

The MC code Geant4/GATE was used to create a detailed model of the Siemens Primus linac head (Siemens AG, Erlangen, Germany). The geometries and compositions of the model were based on the technical drawings provided by the manufacturer as shown in Table 1 that lists the shape, type of the material, thickness, and distances at the material starting point. The model included the beam-line components, such as the bremsstrahlung target, flattening filter, and jaws. The model also included the primary and secondary collimators that directly affect the head leakage and collimator scatter. The components outside the path of the primary beam such as the shielding of the treatment head were not considered in the current model.

Table 1. Specifications of components regarding shape, type of materials, thickness, and distances at material starting point for Siemens Primus linac head.

Description	Traversed material by beam	Thickness (cm)	Distance at material starting point (cm)	Shape
Vacuum envelope assembly	Titanium (Ti)	0.0050	-0.4215	Box
	Water (H_20)	0.0660	-0.3860	Box
	Titanium (Ti)	0.0050	-0.3505	Box
Gap	Air	0.4650	-0.1155	Box
Datum	-	-	0.0000	-
Target	Tungsten	0.0640	0.1490	Box
	Nickel	0.0040	0.1830	Box
	Gold	0.0110	0.1905	Box
	Copper	0.1650	0.2785	Box
	Nickel	0.0015	0.3618	Box
	Gold	0.0035	0.3643	Box
	Stainless Steel	0.1020	0.4170	Box
	Graphite	1.0160	0.9760	Box
	Stainless Steel	0.0040	1.4860	Box
Primary collimator	Tungsten	1.1900	2.2950	Cylinder
	Tungsten	1.1200	3.4500	Cylinder
	Tungsten	1.2400	4.6300	Cylinder
	Tungsten	1.2650	5.8825	Cylinder
	Tungsten	1.5500	7.2900	Cylinder
	Tungsten	1.1930	8.6615	Cylinder
Flattening filter	Stainless Steel	0.3100	7.9100	Cone
	Stainless Steel	0.7635	8.4468	Cone
	Stainless Steel	0.4295	9.0433	Cone
	Stainless Steel	0.0720	9.2940	Cylinder
	Stainless Steel	0.3100	9.4850	Cone
	Stainless Steel	0.4054	9.5327	Cone
X-ray dose chamber	Ceramic (Al_2O_3)	0.1520	10.8100	Cylinder
	Nitrogen (N_2)	0.1840	10.9780	Cylinder
	Ceramic (Al_2O_3)	0.1520	11.1470	Cylinder
	Nitrogen (N_2)	0.1840	11.3150	Cylinder
	Ceramic (Al_2O_3)	0.1520	11.4830	Cylinder
Mirror assembly	Glass	0.2090	16.4985	Box
Lower defining head Y jaws	Tungsten	7.7980	23.5840	Box
Lower defining head X jaws	Tungsten	7.4930	32.0420	Box
Isocenter	-	-	100.0000	-

In Geant4/GATE, electromagnetic (EM) interactions can be simulated using the standard or low-energy packages down to 10 keV [18]. The results of recent studies have revealed that the low-energy package is more appropriate for low-energy photons [19]. In the current study, the simulation was conducted using the standard EM model because it is faster and more efficient in computation than other EM packages. For all simulations, the voxel dimensions were reported as 1×1×1 cm^3. The large size of the voxel helps to reduce the statistical uncertainty of the calculated dose in every voxel as previously stated [12,20]. It was declared that a large voxel size is necessary to simulate doses out of range to achieve reasonable statistical results. As these areas have extremely small doses, this may lead to uncertainty [12,20].

In the present study, the main physical processes implemented in Geant4 for the electron, positron, and photon simulations were bremsstrahlung, Compton scattering, annihilation, gamma conversion (pair production), electron ionization, and photoelectric effect.

Simulation of linac head

In the simulation, each volume was described according to shape, size, position, material composition, and density. The structure was represented by the "world" volume that is a box centered at the origin and should be large enough to include all the volumes involved in the simulation. When any particle escapes from the world volume, its tracking stops. The world volume contains other sub-volumes known as the daughter volumes, and each daughter volume has a certain purpose and name.

The simulation process was divided into two stages for the efficient usage of time. The patient-independent stage agrees with the head of the accelerator on top of the secondary collimator; however, the patient-dependent stage agrees with the simulation for the photon interactions from the secondary collimator to the patient him/herself. The purpose of the first stage was the production of a phase space (PhSp) file [21] as shown in Figure 1. The PhSp stage in Figure 1 includes: electrons, photons, target, primary collimator, flattening filter, monitor chamber, and mirror. The output PhSp file stores all the information (i.e. particle type, direction, three-dimensional [3D] coordinates, production process, weight, and energy) for the incoming particles before the secondary collimator.

Figure 2 depicts the photon spectrum as represented by the PhSp data before the secondary collimator. The resulting PhSp data were later attached to a very thin cylinder of an appropriate diameter just before the secondary collimator and used as photon source as shown in Figure 3. Figure 3 illustrates phase space, X and Y jaws , photons, and water phantom. This second stage was used for the dose calculation in the water phantom.

Detector

The ionization chamber (pinpoint) was the detector used for the relative beam profile measurements in an exceedingly motorized water phantom (model 31016, inner diameters by 2 mm, volume by 0.0160 cm^3, PTW, Germany). It is an extremely small sized ionization chamber with a high spatial resolution for the measurement of high-energy photon beams and is typically recommended to detect the small doses outside the treatment field [22]. The material for the ionization chamber wall is graphite with a protecting acrylic cover.

Linear accelerator

Siemens Primus was the linac used in this study. It is operated at 6 MV up to 200 monitoring units per minute (MU/min). The components of Siemens Primus head linac are shown in Figure 4, including X-ray target, primary collimator, flattening filter, X-ray dose chamber, mirror, secondary collimator (i.e. X and Y jaws), and reticle. The linac head was modeled by the MC simulation to calculate the out-of-field relative doses for comparing to the corresponding measurements.

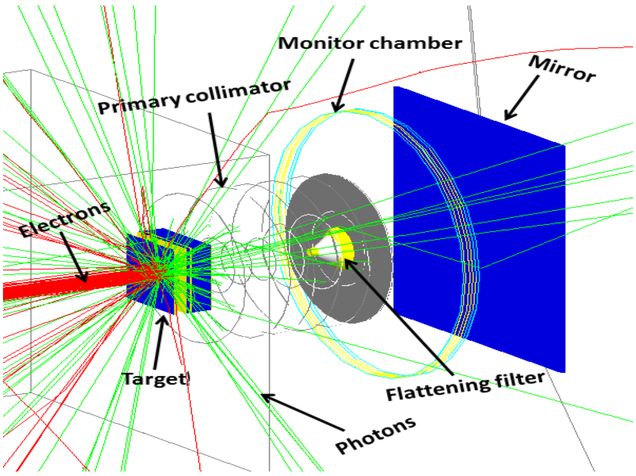

Figure 1. Phase space stage in Monte Carlo simulation showing electrons (red lines), photons (green lines), target block, primary collimator, flattening filter, monitor chamber, and mirror

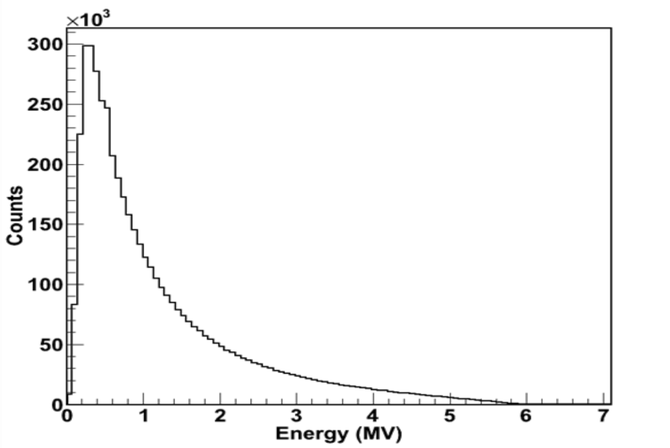

Figure 2. Simulated photon spectrum for energy 6 MV before secondary collimator.

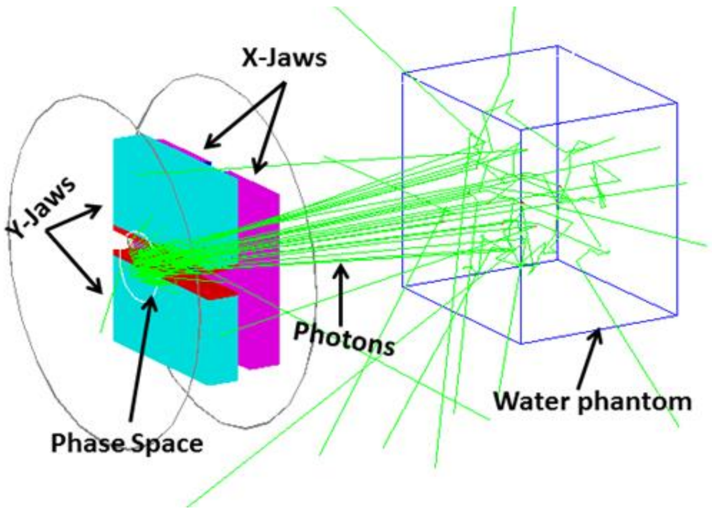

Figure 3. Dose calculation stage in Monte Carlo simulation showing phase space source, X and Y jaws, X-rays beam (green lines), and water phantom.

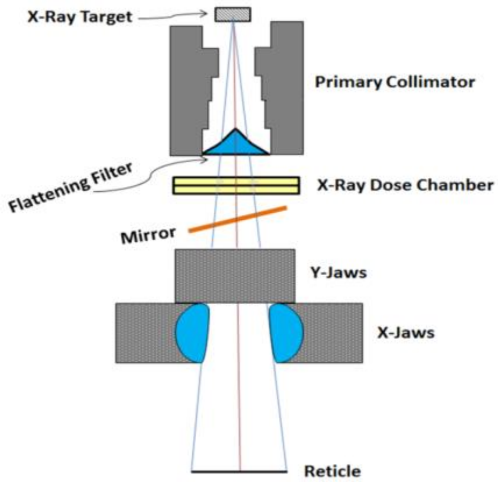

Figure 4. Components of Siemens Primus linac head for 6 MV beam, including X-ray target, primary collimator, flattening filter, X-ray dose chamber, mirror, X and Y jaws, and reticle

Three dimensional water phantoms

A motorized 3D water phantom. The dimensions of this motorized 3D water phantom are 50×50×40 cm^3. Moreover, it encompasses an exactness 3D movement mechanism fabricated from stainless-steel and three stepper motors for the positioning of the detector with a speed of 50 mm/s and positioning accuracy of ±0.1 mm.

The tank is provided with a fast release coupling for a simple communication (Model T 43163). The system involves a cable association box mounted to the tank and the adjustment device for an ionization chamber. It is also attached to the TBA CONTROL UNIT (T41013) and PTW TANDEM (Dual channel electrometer, T10011) for the determination of the dose distributions and analysis of the beams in radiation therapy. The device is controlled by MEPHYSTO mc^2 software (version 3.2.1).

Measurements and simulation conditions

The Measurements were performed on Siemens Primus linac. The output of the linac was set and calibrated before the out-of-field measurements using the IAEA TRS-398 protocol in water phantoms [23]. Out-of-field DPs and percentage depth dose (PDD) curves outside the treatment field were measured using the pinpoint ionization chamber in the water phantom. Out-of-field DPs were measured for field sizes ranging from 5×5 cm^2 to 20×20 cm^2 with an increment of 5 cm. The source to surface distance (SSD) was 100 cm and the ionization chamber was placed at depths of 1.5 (d_{max}), 5.0 and 10.0 cm for each field size, respectively.

Out-of-field DPs were measured for each field size and each depth from the center to 15 cm from the field edge with an increment of 2 mm along the in-plane direction. Each curve was normalized to the measured dose at the central axis (CAX). The PDD curves were measured for the field size 10×10 cm^2 from the surface to 30 cm depth in the water phantom at CAX as a reference and at 5.0 and 7.5 cm from the CAX. Each curve was normalized to the dose at d_{max}.

The coordinates for the accelerator model are outlined in Geant4/GATE as follows: the negative-Z direction expands from the target to the iso-center (i.e., beam-line direction); the negative-X direction expands from the iso-center to the left side of the treatment couch (i.e., cross-plane direction); the negative-Y direction expands from the iso-center to the direction of the gantry (i.e., in-plane direction).

Out-of-field DPs for all considered field sizes at different depths in addition to PDD curves for the field size 10×10 cm^2 at 0.0, 5.0 and 7.5 cm from the CAX were calculated for the simulated water phantom under the same conditions as for the experimental measurements, recommended by the American Association of Physicists in Medicine (AAPM) TG-105. In this regard, it was indicated that the MC simulation should be implemented under the same conditions as for the measurements [8]. However, the simulations were only performed for the PDD curves at 10, 11, 12 and 15 cm from the CAX due to very small unmeasured doses.

For every field size, five runs with 100 M histories were used, and eventually, the average doses were calculated to achieve the best balance between the computation times and uncertainties in low-dose regions. Electron and photon cutoff distances were set to 0.1 mm. The cut-off distance is the distance outside which, particles are no longer tracked or at which the MC simulation stops the transport of the particle if the particle falls outside [10,12].

The comparisons between the measurements and MC simulations are presented in terms of the gamma index [24]. The gamma index is the most suitable parameter to indicate the accuracy of the simulation for the out-of-field dose regions due to the high dose gradient and large dose differences that appear. The gamma index evaluation considers both the dose difference and distance to agreement (DTA) comparisons. The dose difference represents the difference of point-to-point doses between the calculated results and measured data. However the DTA is the distance between the measured point and nearest one in the simulated dose distribution with a similar dose. The gamma function is obtained by the following equation:

$$\Gamma(\vec{r}_s,\vec{r}_m) = \sqrt{\frac{r^2(\vec{r}_s,\vec{r}_m)}{\Delta d^2} + \frac{\delta^2(\vec{r}_s,\vec{r}_m)}{\Delta D^2}} \quad (1)$$

where $\vec{r}_m$ is the position vector of the measured points, $\vec{r}_s$ is the position vector of the calculated points by simulation, Δd is the DTA criterion and ΔD is the dose difference criterion. These criteria are deduced from the voxel sizes and dose uncertainties in the MC simulations in addition to the ionization chamber dimensions, measured position and dose errors. The equation $r(\vec{r}_s,\vec{r}_m) = |\vec{r}_s - \vec{r}_m|$ denotes the distance between the simulation and measured points, and the equation $\delta(\vec{r}_s,\vec{r}_m) = D_s(\vec{r}_s) - D_m(\vec{r}_m)$ indicates the difference between the dose values of the simulated and measured points. Then the γ index is obtained from the following equation:

$$\gamma(\vec{r}_m) = \min\{\boldsymbol{\Gamma}(\vec{r}_s,\vec{r}_m)\} \,\forall\, \{\vec{r}_s\} \quad (2)$$

If $\gamma(\vec{r}_m) \leq 1$, the calculation passes the criteria for each measured point; nevertheless, if $\gamma(\vec{r}_m) > 1$, the calculation does not meet the acceptance criteria. The gamma passing rate is defined as the matching percentage between the measurement and MC simulation. It is calculated as the percentage ratio between the number of points with gamma indices less than or equal one to the total number of points.

In this study, the pre-defined acceptance criteria of gamma passing rates adjusted for the dose difference and DTA criteria were 5% and 5 mm for all the out-of-field DPs, 2% and 2 mm for the PDD on the CAX, as well as 10% and 10 mm for the PDD at 5.0 and 7.5 cm from the CAX. These criteria were selected to increase the efficiency of the output results statistically.

Results

Figures 5-8 depict the comparisons between the measurements and MC simulations with the associated gamma indices for the out-of-field DPs as a function of distance from the CAX along the in-plane direction for field sizes of 5×5, 10×10, 15×15 and 20×20 cm^2 at depth 10 cm. The comparisons show very agreement between the measured and simulated doses for all field sizes and different depths in terms of the gamma passing rates for the out-of-field DPs along the in-plane direction as listed in Table 2.

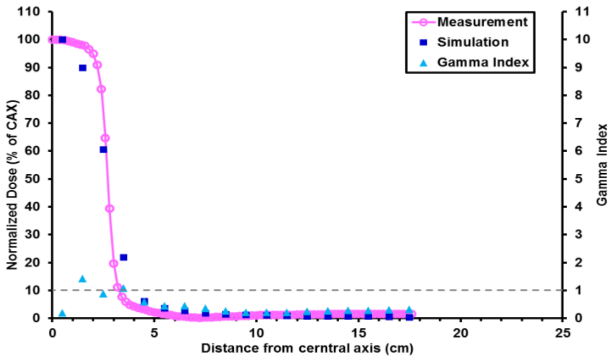

Figure 5. Out-of-field dose profile for 5×5 cm^2 field size at 10.0 cm depth along in-plane direction with corresponding gamma indices for measurements and Monte Carlo simulations.

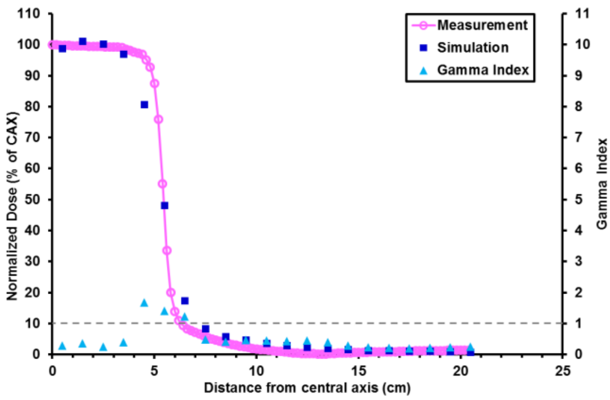

Figure 6. Out-of-field dose profile for 10×10 cm^2 field size at 10.0 cm depth along in-plane direction with corresponding gamma indices for measurements and Monte Carlo simulations.

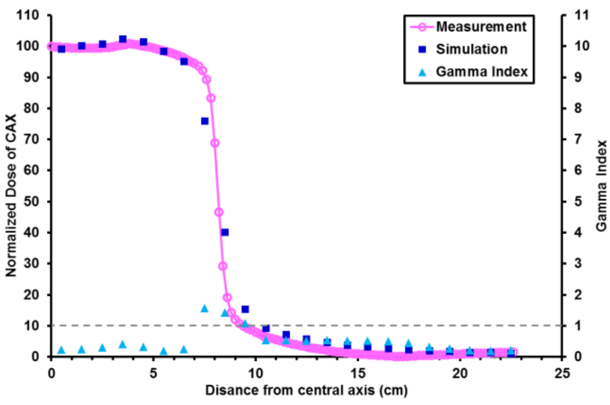

Figure 7. Out-of-field dose profile for 15×15 cm^2 field size at 10.0 cm depth along in-plane direction with corresponding gamma indices for measurements and Monte Carlo simulations.

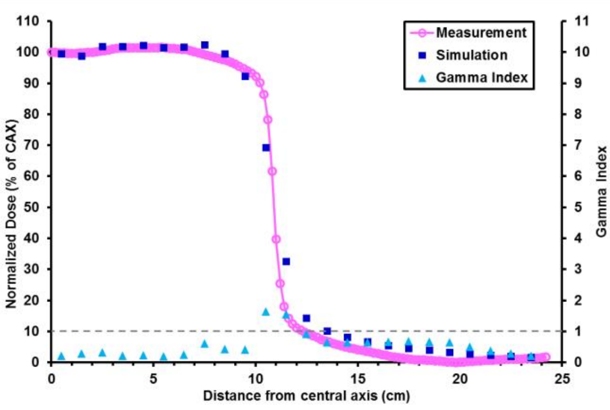

Figure 8. Out-of-field dose profile for 20×20 cm^2 field size at 10.0 cm depth along in-plane direction with corresponding gamma indices for measurements and Monte Carlo simulations.

Comparisons between the measurements and MC simulations for the in-field and out-of-field PDD curves along the in-plane direction for field size 10×10 cm^2 from the surface down to 30 cm depth are shown in figures 9-11 on the CAX, as well as at 5.0 and 7.5 cm off axis.

Table 2. Gamma passing rates for out-of-field dose profiles for field sizes 5×5, 10×10, 15×15 and 20×20 cm^2 at depths 1.5, 5.0 and 10.0cm for each dose profile.

Field size (cm^2)	Depth (cm)	Gamma passing rate (%)
	1.5	83.30
5×5	5.0	83.30
	10.0	89.50
	1.5	95.00
10×10	5.0	90.50
	10.0	86.40
	1.5	86.96
15×15	5.0	91.67
	10.0	88.00
	1.5	95.83
20×20	5.0	91.67
	10.0	91.67

Table 3. Gamma passing rates for out-of-field percentage depth dose curves at 0.0, 5.0 and 7.5 cm from central axis

Distance from central axis (cm)	Gamma passing rate (%)
0.0	100.00
5.0	100.00
7.5	76.70

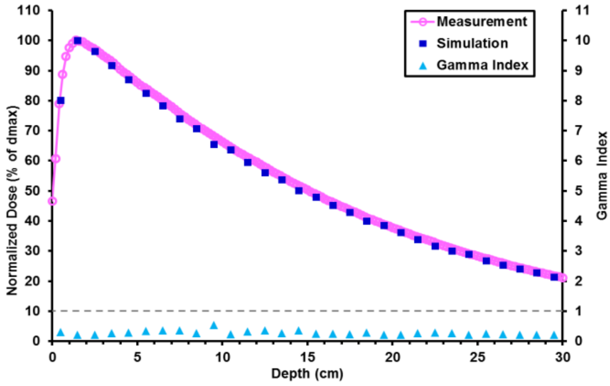

Figure 9. Out-of-field percentage depth dose along in-plane direction for field size 10×10 cm2 on central axis in water phantom with corresponding gamma indices for measurements and Monte Carlo simulations.

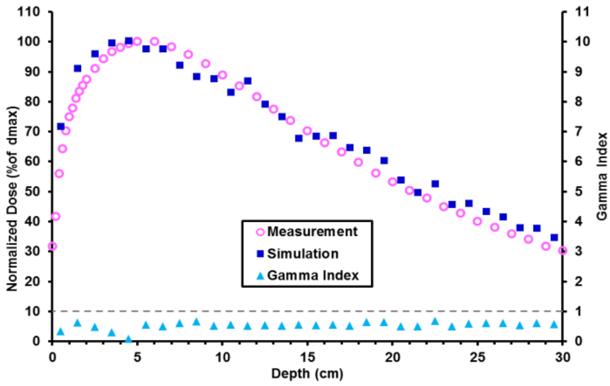

Figure 10. Out-of-field percentage depth dose along in-plane direction for field size 10×10 cm2 at 5.0 cm from central axis in water phantom with corresponding gamma indices for measurements and Monte Carlo simulations.

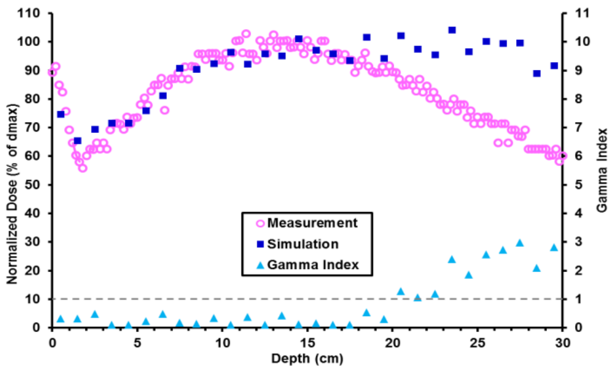

Figure 11. Out-of-field percentage depth dose along in-plane direction for field size 10×10 cm2 at 7.5 cm from central axis in water phantom with corresponding gamma indices for measurements and Monte Carlo simulations.

The comparisons between the measurements and MC simulations demonstrated agreement for the PDD curves on the CAX and at 5.0 cm off axis. However, there was a slight disagreement between the measurements and simulations for the PDD curve at 7.5 cm off axis, especially at depths greater than about 20 cm. The gamma passing rates for the out-of-field PDD curves along the in-plane direction for field size 10×10 cm^2 at 0.0, 5.0 and 7.5 cm off axis are listed in Table 3.

Figure 12 shows the simulated out-of-field PDD curves along the in-plane direction for field size 10×10 cm2 from the surface down to 30 cm depth in the water phantom at 10, 11, 12 and 15 cm off axis. It is worth noting that almost all the out-of-field PDD curves had a similar trend shape at distances ≥ 10 cm off axis.

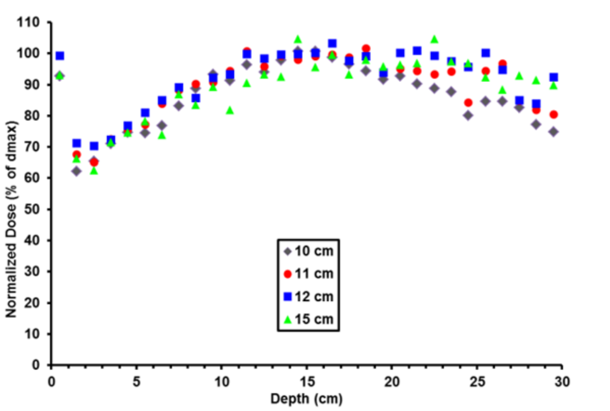

Figure 12. Simulated out-of-field percentage depth dose curves along in-plane direction for field size 10×10 cm2 at 10, 11, 12 and 15 cm from central axis.

Discussion

The validation for the in-field doses using a similar MC model for Siemens Oncor was reported in another recent study [25]. The new comparisons between the experimental measurements and MC simulations for the out-of-field DPs along the in-plane direction showed agreement for all the field sizes at different depths. The gamma passing rates of the DPs were 83.30%, 83.30% and 89.50% for 5×5 cm^2, 95.00%, 90.50% and 86.40% for 10×10 cm^2 , 86.96%, 91.67% and 88.00% for 15×15 cm^2 ,and 95.83%, 91.67% and 91.67% for 20×20 cm^2 at depths of 1.5, 5.0 and 10.0 cm respectively.

According to the comparisons between the measurements and simulation for all field sizes in Figures 5-8, it was noticed that the MC simulation slightly overestimated the out-of-field doses, compared to the measurements.

Based on the values of gamma passing rates for the out-of-field DPs, it was remarked that the best agreement between the measurements and simulations was achieved for the largest field size 20×20 cm^2. The number of points passing the criteria decreased as the field size reduced where the least agreement was observed for the field size 5×5 cm^2. This is due to the increasing number of points with doses lower than 20% of the maximum dose in the out-of-field region for the smallest field size. However, in larger field sizes, there were higher contributions of photons in the out-of-field region that improved the overall gamma passing rates. These results are consistent with the findings of Joosten et al. result [26] who showed that the matching percentage values between the measurements and MC simulations are higher for larger fields than smaller fields. Finally Joosten et al. concluded that their model can be generically used for open fields (≥10×10 cm^2).

The present study included the measurements and MC simulations for PDD curves for field size 10×10 cm^2 at 0.0, 5.0 and 7.5 cm off axis followed by making a comparison through the gamma index technique to investigate the gamma passing rates between the measurements and the simulations. The comparisons showed agreement between the measurements and MC simulations for PDD curves at CAX and 5.0 cm off axis. The two curves almost had identical trends where the dose increased until a certain d_{max} and then decreased gradually.

Nevertheless, the PDD curve at 7.5 cm off axis had a different behavior revealing a dose increase near the surface from the contaminating electrons outside the field. It was also noticed that the agreement was valid until nearly a depth of 20cm in the water phantom. However, at depths greater than about 20 cm, it was observed that the MC simulation tended to overestimate the measured dose. To better understand this phenomenon, the loss in the ionization chamber efficiency should be considered for the detection a huge number of photons with extremely low energies at this large depth. On the other hand, the doses from all these low energy photons are still added together in the MC simulations to some extent.

In a study carried out by Almberg [27], an MC model was developed using the BEAMnrc MC code for the Elekta Synergy linac, and an agreement was verified between the measurements and MC simulations for the out-of-field PDD curves for half-beam blocked 10×10 cm^2 from 2 to 25 cm depth only at 8.5 cm off axis with percentage (96.70%). This matching percentage value is inconsistent with the percentage value of the present study (76.70%). This difference is believed to be due to using half-beam blocked field size in the aforementioned study that helps to avoid beam divergence, leading to an out-of-field PDD curve at a constant distance from the field edge. In addition, the out-of-field PDD curve was only from 2 to 25 cm depth.

In the present study, the normal beam radiation with divergence was used indicating that, no half-beam blocked the field, and the out-of-field PDD curve was from the surface down to 30 cm depth. As previously mentioned, the mismatch between the measurements and simulations occurred at depths greater than about 20 cm. Consequently, the observed difference between measurements and simulation could also be due to the beam divergence that increases at large depths resulting in unequal distances from the field edge at each depth leading to lack of regularity for the dose distribution. This effect was clearer in the MC simulations due to the very great uncertainties at these great depths for very low doses.

The present study also included the PDD curves outside the treatment field at 10, 11 12 and 15 cm off axis; however, these curves were calculated by the MC simulations only due to the difficulty associated with the experimental measurements that are time-consuming and require very special and more sensitive measuring equipment suitable for very low doses in the out-of-field region. The simulated curves showed a similar trend for all the considered distances from the CAX ≥ 10cm where the dose increased near the surface due to the contaminating electrons outside the fields as mentioned earlier; then, it decreased quickly followed again by a gradual increase.

For all field sizes, although the matching percentage between the simulated and measured doses in the present study was not generally 100%, there is a more reasonable agreement for the out-of-field doses since these lower values were expected in several previous studies [12, 20] and since the out-of-field regions have very low radiation doses. Consequently, this leads to large uncertainties in the simulation and measurement which are unavoidable.

The results of the present study are consistent with the findings of Kry et al. [12]. They compared the measured out-of-field doses using thermo-luminescent dosimeter (TLD) at several distances from the CAX to 55 cm for a Varian 2100 accelerator operating at 6 MV with those simulated by an MC model (i.e., MCNPX). In addition, the matching percentage between the measurements and MC simulations was 84.00% on average.

The results of the present study are also in line with the findings of a study by Bednarz et al. [10]. They validated an MC model using the MCNPX code to calculate the out-of-field absolute doses for all field sizes form the center of the treatment field to distances less than 60 cm off axis at depths of $d_{\max}$, as well as 5 and 10 cm for Varian Clinac accelerator operating at 6 MV. The matching percentages were 89.30% - 93.80% , 66.00% - 85.80% , and 70.00% - 79.00% for 20×20, 10×10, and 4×4 cm^2 respectively. They also showed that the matching percentage values between the measurements and MC simulations were better for large fields than small fields.

The slight differences in the agreement between the results of this study and findings of other studies are mostly due to the different linac models and MC codes. This statement was mentioned by Kry et al. [12] who concluded that the out-of-field dose level far from the treatment field, where leakage radiation dominates, may be different by a factor of 3 or more in the comparison between the Varian 2100 and Siemens Primus linacs. In addition, the present study also included the out-of-field doses only up to 15 cm from the treatment field edge, and this constraint is based on the findings of Kry et al. [28]. They stated that the accuracy in the beam-line components model for the out-of-field doses can be achieved up to ~15cm from the field edge; however, at greater distances, the accuracy becomes worse.

The dose measurements in the water phantom cannot be performed for the whole distance from the CAX to the phantom wall (25 cm) due to the limited mechanicals movement of the ion chamber. Only doses from the CAX up to a horizontal distance of about 24 cm along the in-plane direction can be measured. This limitation indicated that the out-of-field PDD for the field size 20×20 cm^2 can only be measured through the additional distances of about 14 cm only from the field edge at 10 cm up to about 24 cm from the CAX.

There are some hardware devices clinically used in front of the therapeutic beam that may affect the out-of-field doses and consequently the generation of SCs. Joosten et al. [29] evaluated the out-of-field doses for breast cancer patients with different techniques, including two-dimensional radiation therapy (2DRT), three-dimensional conformal radiation therapy (3DCRT) and intensity modulated radiation therapy (IMRT) using MC simulations (BEAMnrc) and compared the results with a commercial treatment planning system (TPS). The results showed that the out-of-field doses from the 3DCRT technique using external wedges were higher than the 2DRT and IMRT techniques.

However, the present study did not include any clinical cases or hardware devices in front of the therapeutic beam. All the used beams were open fields in the water phantom to facilitate the validation of the MC model for the Siemens 6 MV photon beam with minimal configuration as an essential requirement before any proposed future study to confidently simulate the out-of-field doses for actual clinical patients in real clinical conditions.

On the other hand, Diallo et al. [30] observed that the majority of SCs were located in the region of the beam-bordering, and out of 115 SCs, only 9 cases may occur at distances located higher than 20 cm away from the beam border. Out of these nine SCs, there was a melanoma with no direct evidence confirming its association with radiation [31]. Recently, the results of, one of the important studies on SC risk after breast radiotherapy; revealed the statistically raising of SC risks for organs located near the treated breast, such as the lungs, esophagus, pleura, contralateral breast, and chest sarcomas [32].

Nonetheless, there was no statistical evidence on any rising risk of SC for organs located further away from the radiotherapy beams used for breast radiotherapy. Therefore, it is recommended to perform further studies to develop and validate a more detailed MC model for Siemens Primus linac operated at 6 MV or higher photon energies based on adding the missing structural and shielding components that surround the beam-line components. Consequently, the small out-of-field dose for distances greater than 15 cm from the field edge can be better studied and verified in this regard.

Conclusion

In this study, a new MC model was validated using the Geant4/GATE code to calculate the out-of-field doses for 6 MV Siemens Primus linac. The model achieved an agreement with measurements for all considered field sizes from the center of the treatment field to 15 cm from the field edge and for all depths less than about 20 cm. For depths greater than 20 cm, it was noticed that the MC simulation tended to overestimate the dose.

The new MC model in the present study can be considered as an adequate approach for the assessment of the PDDs at distances ≥ 10 cm off axis that cannot be precisely measured.

The MC linac model validated in the current study can also be used in future studies to evaluate the doses in the out-of-field organs for real clinical cases and consequently estimate the risks of radiation-induced SCs. For this purpose, the computed tomography (CT) scans of patients can be directly implemented in the MC model instead of using a geometrical water phantom. This suggested study should avoid the laborious experimental dose measurements in anthropomorphic phantoms which are very time-consuming.

Acknowledgment

The authors would like to thank "Mit Ghamr Oncology Center" for its generous cooperation with this study. The authors would also like to extend their gratitude to Eng. Mohamed Osama, a biomedical engineer and president of On-medical Company for his great efforts in this project.

References

1. Xu X , Bednarz B, Paganetti H. A review of dosimetry studies on external-beam radiation treatment with respect to second cancer induction. Physics in Medicine & Biology.2008; 53(13):R193.
2. Stovall M, Blackwell C, Cundiff J, Novack D, Palta J, Wagner LK et al. Fetal dose from radiotherapy with photon beams: report of AAPM Radiation Therapy Committee Task Group No. 36. Medical physics. 1995;22(1):63-82.
3. Wilde G , Sjöstrand J. A clinical study of radiation cataract formation in adult life following γ irradiation of the lens in early childhood. British journal of ophthalmology.1997;81(4):261-6.
4. Preston DL, Shimizu Y, Pierce DA, Suyama A, Mabuchi K. Studies of mortality of atomic bomb survivors. Report 13: Solid cancer and noncancer disease mortality: 1950‐1997. Radiation research. 2003 Oct;160(4):381-407.
5. Brenner D, Rochelle E, Eric J, Elaine R . Second malignancies in prostate carcinoma patients after radiotherapy compared with surgery. Cancer: Interdisciplinary International Journal of the American Cancer Society. 2000; 88(2):398-406.
6. Elgendy RA , Attia WM , Attalla EM, Elnaggar MA. Influence of Distinct Radiotherapy Techniques to Induce Second Cancer Risks in Left Breast Cancer. Oncology. 2018;7:193-202.
7. Sungkoo CH, Seong Hoon KI, Chan Hyeong KI, Jang Guen JH. Secondary cancer risks in out-of-field organs for 3-D conformal radiation therapy. Prog. Nucl. Sci. Technol. 2011; 1:512-24.
8. Chetty IJ, Curran B, Cygler JE, DeMarco JJ, Ezzell G, Faddegon BA, et al. Report of the AAPM Task Group No. 105: Issues associated with clinical implementation of Monte Carlo-based photon and electron external beam treatment planning. Medical physics. 2007;34(12): 4818-53.
9. Jabbari K, Anvar H, Tavakoli M, Amouheidari A. Monte carlo simulation of siemens oncor linear accelerator with beamnrc and dosxyZnrc code. Journal of medical signals and sensors. 2013;(3.3):172.
10. Bednarz B, Xu X. Monte Carlo modeling of a 6 and 18 MV Varian Clinac medical accelerator for in-field and out-of-field dose calculations: development and validation. Physics in Medicine & Biology. 2009;54(4):N43.
11. Chiban O, Charlie C. On the discrepancies between Monte Carlo dose calculations and measurements for the Varian photon beam. Medical physics. 2007;34(4):1206-16.
12. Kry SF, Titt U, Pönisch F, Followill D, Vassiliev ON, Allen White R, et al. A Monte Carlo model for calculating out-of-field dose from a Varian beam. Medical physics. 2006; 33(11):4405-13.
13. Visvikis D, Bardies M, Chiavassa S, Danford C, Kirov A, Lamare F, et al. Use of the GATE Monte Carlo package for dosimetry applications. Nuclear Instruments and Methods in Physics Research Section A: Accelerators, Spectrometers, Detectors and Associated Equipment. 2006;569(2):335-40.
14. The Geant4 web site , http://www.opengatecollaboration.org/UsersGuide
15. Jan S, Santin G, Strul D, Staelens S, Assie K, Autret D, et al. GATE: a simulation toolkit for PET and SPECT. Physics in Medicine & Biology. 2004 Sep 10;49(19):4543.
16. De Beenhouwer J, Staelens S, Vandenberghe S, Verhaeghe J, Van Holen R, Rault E, et al. Physics process level discrimination of detections for GATE: assessment of contamination in SPECT and spurious activity in PET. Medical physics. 2009;36(4):1053-60.
17. Agostinelli S, Allison J, Amako KA, Apostolakis J, Araujo H, Arce P, et al. Geant4—a simulation toolkit. Nuclear instruments and methods in physics research section A: Accelerators, Spectrometers, Detectors and Associated Equipment. 2003;506(3):250-303.
18. Elles S, Ivanchenko VN, Maire M, Urban L. Geant4 and Fano cavity test: where are we?. In Journal of Physics: Conference Series. 2008;102(1) 012009.
19. Faddegon BA , Asai M, Perl J, Ross C, Sempau J, Tinslay J, etal. Benchmarking of Monte Carlo simulation of bremsstrahlung from thick targets at radiotherapy energies. Medical physics. 2008;35(10):4308-17.
20. Kry SF, Titt U, Followill D, Pönisch F, Vassiliev ON, White RA, et al. A Monte Carlo model for out-of-field dose calculation from high-energy photon therapy. Medical physics. 2007;34(9):3489-99.
21. Brun R, Rademakers F. ROOT—an object oriented data analysis framework. Nuclear Instruments and Methods in Physics Research Section A:

Accelerators, Spectrometers, Detectors and Associated Equipment. 1997;389(1-2): 81-86.

22. Abdelaal AM., Attalla EM, Elshemey WM. Dose estimation outside radiation field using Pinpoint and Semiflex ionization chamber detectors. Radiation Physics and Chemistry. 2017; 139:120-5.
23. Technical Report Series (TRS) No. 398 Absorbed dose determination in external beam radiotherapy- An international code of practice for dosimetry based on standards of absorbed dose to water. 2000.
24. Low DA, Harms WB, Mutic S, Purdy JA. A technique for the quantitative evaluation of dose distributions. Medical physics. 1998;25(5):656-61.
25. Ibrahim HF, Fahmy AM, Attalla EM. Assessment of Radiation Doses in A Medical Linear Accelerator Using Simulation Models and Experimental Verification. Isotope and Radiation Research. 2017;49(1):165-78.
26. Joosten A, Bochud F, Baechler S, Levi F, Mirimanoff RO, Moeckli R. Variability of a peripheral dose among various linac geometries for second cancer risk assessment. Physics in Medicine & Biology. 2011;56(16):5131.
27. Almberg SS, Frengen J, Lindmo T. Monte Carlo study of in-field and out-of-field dose distributions from a linear accelerator operating with and without a flattening-filter. Medical physics. 2012;39(8):5194-203.
28. Kry SF, Bednarz B, Howell RM, Dauer L, Followill D, Klein E, et al. AAPM TG 158: measurement and calculation of doses outside the treated volume from external-beam radiation therapy. Medical physics. 2017;44(10):391-429.
29. Joosten A , Matzinger O, Jeanneret-Sozzi W, Bochud F, Moeckli R. Evaluation of organ-specific peripheral doses after 2-dimensional, 3-dimensional and hybrid intensity modulated radiation therapy for breast cancer based on Monte Carlo and convolution/superposition algorithms: implications for secondary cancer risk assessment. Radiotherapy and Oncology. 2013;106(1):33-41.
30. Diallo I, Haddy N, Adjadj E, Samand A, Quiniou E, Chavaudra J, et al. Frequency distribution of second solid cancer locations in relation to the irradiated volume among 115 patients treated for childhood cancer. International Journal of Radiation Oncology* Biology* Physics. 2009;74(3):876-83.
31. Little MP, Hoel DG, Molitor J, Boice Jr JD, Wakeford R, Muirhead CR. New models for evaluation of radiation-induced lifetime cancer risk and its uncertainty employed in the UNSCEAR 2006 report. Radiation research. 2008;169(6):660-76.
32. De Gonzalez AB, Curtis RE, Gilbert E, Berg CD, Smith SA, Stovall M, et al. Second solid cancers after radiotherapy for breast cancer in SEER cancer registries. British journal of cancer. 2010;102(1):220-6.